

QVD: Post-training Quantization for Video Diffusion Models

Shilong Tian*[†]
tianshilong@buaa.edu.cn
Beihang University

Hong Chen*
18373205@buaa.edu.cn
Beihang University

Chengtao Lv*
lvchengtao@buaa.edu.cn
Beihang University

Yu Liu
Beihang University

Jinyang Guo
Beihang University

Xianglong Liu
Beihang University

Shengxi Li
Meituan

Hao Yang
Meituan

Tao Xie
Meituan

ABSTRACT

Recently, video diffusion models (VDMs) have garnered significant attention due to their notable advancements in generating coherent and realistic video content. However, processing multiple frame features concurrently, coupled with the considerable model size, results in high latency and extensive memory consumption, hindering their broader application. Post-training quantization (PTQ) is an effective technique to reduce memory footprint and improve computational efficiency. Unlike image diffusion, we observe that the temporal features, which are integrated into all frame features, exhibit pronounced skewness. Furthermore, we investigate significant inter-channel disparities and asymmetries in the activation of video diffusion models, resulting in low coverage of quantization levels by individual channels and increasing the challenge of quantization. To address these issues, we introduce the first PTQ strategy tailored for video diffusion models, dubbed **QVD**. Specifically, we propose the **High Temporal Discriminability Quantization (HTDQ)** method, designed for temporal features, which retains the high discriminability of quantized features, providing precise temporal guidance for all video frames. In addition, we present the **Scattered Channel Range Integration (SCRI)** method which aims to improve the coverage of quantization levels across individual channels. Experimental validations across various models, datasets, and bit-width settings demonstrate the effectiveness of our QVD in terms of diverse metrics. In particular, we achieve near-lossless performance degradation on W8A8, outperforming the current methods by 205.12 in FVD.

CCS CONCEPTS

• **Computing methodologies** → **Artificial intelligence**.

KEYWORDS

post-training quantization, video diffusion models, multimodal

*Equal contribution.

[†]Work done as an intern at Meituan.

Permission to make digital or hard copies of all or part of this work for personal or classroom use is granted without fee provided that copies are not made or distributed for profit or commercial advantage and that copies bear this notice and the full citation on the first page. Copyrights for components of this work owned by others than the author(s) must be honored. Abstracting with credit is permitted. To copy otherwise, or republish, to post on servers or to redistribute to lists, requires prior specific permission and/or a fee. Request permissions from permissions@acm.org.

ACM MM, 2024, Melbourne, Australia

© 2024 Copyright held by the owner/author(s). Publication rights licensed to ACM.

ACM ISBN 978-x-xxxx-xxxx-x/YY/MM

<https://doi.org/10.1145/nnnnnnn.nnnnnnn>

1 INTRODUCTION

The diffusion model has experienced vigorous development in vision generation tasks due to its high controllability, photorealistic generation, and impressive diversity. Recently, research on video tasks based on diffusion models has gained increasing attention, driving the emergence of numerous attractive applications including, but not limited to, text-to-video [5, 18, 20, 65], image-guided video generation [4, 18, 25, 44], video editing [14, 41, 59], and other conditionally guided video generation tasks [53, 54, 60].

Despite the remarkable effects of diffusion models, their relatively slow inference speed and substantial memory usage have hindered their broader application, particularly in video tasks. The core reasons for these limitations include: 1) The denoising procedure encompasses several hundred iterations, and 2) The extension of frame dimensions results in a notable escalation in memory utilization compared with image diffusion models. There are primarily two strategies to overcome such bottlenecks: minimizing the number of iteration steps, including [37, 51], and optimizing the efficiency of individual denoising operations through techniques like pruning [16, 32], distillation [30, 39], or quantization [33, 47]. The former only focuses on the first issue while ignoring the significant memory consumption. In this work, we mainly study the quantization of video diffusion models.

Model quantization is a widely adopted and practical approach for reducing model footprint and accelerating inference by mapping floating-point values into low-bit integers. Among various quantization methods, post-training quantization (PTQ) requires no retraining or fine-tuning of the model and incurs minimal overhead, making it more practical in deployment. PTQ methods have been extensively studied in image diffusion models [19, 27, 33, 47, 49]. However, these methods exhibit significant performance degradation when directly applied to video diffusion models. We discover that the rationale lies in two aspects, *i.e.*, the introduction of the frame dimensions and temporal attention modules in video diffusion models. Specifically, based on the following two observations, we explore the difficulty of quantization for VDMs:

Observation 1: Highly reliant on discriminable temporal features. As illustrated in Figure 1(a), in a single denoising iteration, the features of all frames rely on the same temporal feature, which implies that disturbances arising from the quantization of temporal features will impact the generative quality of all frames. Furthermore, we observe that the uniform quantizer leads to the homogenization of temporal features, demonstrating a significant performance gap compared to those utilizing full-precision temporal features. Upon

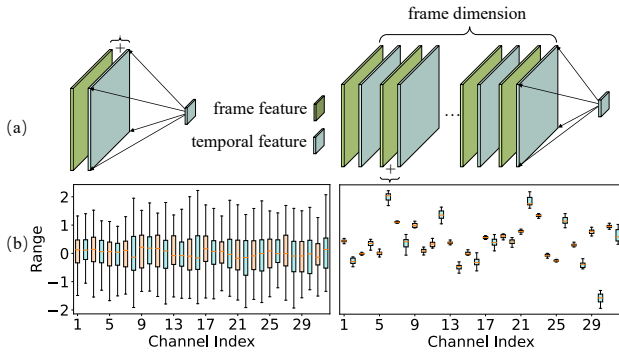


Figure 1: Comparison of image diffusion (left) and video diffusion (right). (a) Features of all frames rely on the same temporal feature in VDMs. (b) Significantly inter-channel variation issue occurs in temporal attention modules.

analyzing the distribution of temporal features, we observe a pronounced skewness near zero, where outliers often exceed thousands of times the magnitude of regular values, making conventional uniform quantizers unsuitable for temporal features.

Observation 2: Inter-channel variations reduce the coverage of quantization levels. As depicted in Figure 1(b), in the image diffusion model, activation across different channels tends to be concentrated, with the range of activation for individual channels closely approximating the range of overall activation. Each channel covers nearly all quantization levels, indicating low quantization difficulty. In contrast to the image diffusion model, the activation values of the temporal attention module in video diffusion models are discrete and asymmetric across channels. The range of individual channels is significantly narrower than the overall activation. As a result, each channel accesses only a tiny fraction of quantization levels, posing a new challenge for PTQ.

To tackle these obstacles, we propose **QVD**, the first post-training quantization scheme for video diffusion models. Figure 2 shows the overall pipeline of the QVD. To mitigate the problem in observation 1, we introduce the **High Temporal Discriminability Quantization (HTDQ)**, which contains a **High Discriminability Temporal Quantizer (HiDi-TQ)** to prioritize numerous near-zero values and retains high identifiability of time, and the **Temporal Discriminability score (TDScore)** to evaluate the similarity of adjacent temporal features. To settle the issue in observation 2, we introduce a **Scattered Channel Range Integration (SCRI)** method, which employs a per-channel integration operation to enhance the coverage of quantization levels by individual channels, therefore handle the discrete range of activations. We conduct comprehensive experiments to validate the superiority and versatility of our QVD.

In summary, our contributions are as follows:

- We propose **QVD** quantization framework, which, to our knowledge, is the first PTQ method tailored explicitly for video diffusion models.
- We identify the critical inter-channel variations issue in video diffusion models and highlight the significance of accurate and discriminable temporal features for video generation.

- We introduce **SCRI** to improve the coverage of quantization levels across individual channels, **TDScore** to quantify temporal similarity, and the **HiDi-TQ** quantizer to keep high discriminability of temporal features.
- Extensive experiments on various models and datasets demonstrate the superiority of QVD, which results in a 257.9 decrease in the FVD for the W6A8 PTQ of video diffusion models compared to existing methods in the image domain.

2 RELATED WORK

2.1 Video Diffusion

Recently, Diffusion Probabilistic Models [22, 50] have overtaken Generative Adversarial Networks (GANs) [13] as the leading approach in generative modeling, establishing a new benchmark for the field. Following the success of image diffusion techniques, video diffusion has also received widespread interest. VDM [23] becomes the pioneer in video generation and adopts 3D U-Net [12] structure. Some text-to-video (T2V) methods, such as MagicVideo [64], LVDM [21] utilize the Latent Diffusion Model (LDM) [46] and plug temporal modeling technique to it. Subsequent T2V schemes [5, 55, 55, 62] extend the single-stage to multi-stages. Image-to-video (I2V) methods, as another promising scheme, generate the video from a conditional image. Initially, LaMD [26] focuses on training an auto-encoder to isolate motion information contained in videos. Stable Video Diffusion leverages text-to-image pretraining, video pretraining, and high-quality video finetuning to produce high-resolution videos. AnimateDiff [18] integrates the LoRA [24] and avoids the time-consuming retraining. Other conditions, such as pose [29, 38], motion [7, 61], sound [31, 36] are also proposed. Substantial efficient solutions, including retraining-free sampler [2, 35, 37] and retraining-based methods [51, 63]. The first aims to decrease the number of sampling steps and the second is time-consuming. However, there is a gap in the research on video diffusion, and our work is the first to undertake a study in this area.

2.2 Quantization

Quantization has achieved substantial advancements in the domain of neural network acceleration, as corroborated by numerous scholarly investigations [6, 10, 28, 34, 40, 42, 56, 58]. Mainstream quantization schemes can be briefly classified into two categories: quantization-aware training (QAT) [9, 15] and post-training quantization (PTQ) [6, 10, 40]. QAT aims to retrain the network on the whole dataset, while PTQ only requires a small amount of unlabeled datasets for calibration. Several classical quantization methods, such as MinMax [28], Percentile [58], LSQ [15], PACT [9] are proposed successively for the convolutional neural networks. In recent years, the quantization of diffusion models [19, 27, 33, 47] has garnered widespread attention within the academic community. PTQ4DM [47] first discovers the difficulty of multiple-step activation distribution and generates the calibration data from a kew-normal distribution. Q-diffusion [33] introduces the uniform sampling calibration and split shortcut quantization for the bimodal activation distribution of the shortcut layers. PTQD [19] decomposes the quantization noise into interrelated and residual parts. TFMQ-DM [27] addresses the temporal feature disturbance and optimizes them separately. However, these existing methods mainly focus on image diffusion. In comparison, video

diffusion necessitates significantly greater computational resources and storage. To the best of our knowledge, our work is the first to conduct the quantization for video diffusion models.

3 PRELIMINARIES

3.1 Diffusion Models

Diffusion models employ a sophisticated approach to image generation, relying on the application of Gaussian noise through a Markov chain in a forward process and a learned reverse process to generate high-quality images. Beginning with an initial data sample $\mathbf{x}_0 \sim q(\mathbf{x})$ from a real distribution $q(\mathbf{x})$, the forward diffusion process incrementally adds Gaussian noise over T steps:

$$q(\mathbf{x}_t | \mathbf{x}_{t-1}) = \mathcal{N}(\mathbf{x}_t; \sqrt{1 - \beta_t} \mathbf{x}_{t-1}, \beta_t \mathbf{I}), \quad (1)$$

where t is an arbitrary timestep and $\{\beta_t\}$ is the variance schedule. The reverse process, in contrast, aims to denoise the Gaussian noise $x_T \sim \mathcal{N}(0, \mathbf{I})$ into the target distribution by estimating $q(\mathbf{x}_{t-1} | \mathbf{x}_t)$. In every step of the reverse process, marked by t , the model estimates the conditional probability distribution using a network $\epsilon_\theta(\mathbf{x}_t, t)$, which incorporates both the timestep t and the prior output \mathbf{x}_t as its inputs:

$$\begin{aligned} x_{t-1} &\sim p_\theta(x_{t-1} | x_t) = \\ &\mathcal{N}\left(x_{t-1}; \frac{1}{\sqrt{\alpha_t}} \left(x_t - \frac{1 - \alpha_t}{\sqrt{1 - \bar{\alpha}_t}} \epsilon_\theta(\mathbf{x}_t, t)\right), \beta_t \mathbf{I}\right), \end{aligned} \quad (2)$$

where $\alpha_t = 1 - \beta_t$ and $\bar{\alpha}_t = \prod_{i=1}^t \alpha_i$. When extending the image diffusion to video diffusion, the latent noise adds a new dimension K which denotes the length of the video frames.

3.2 Model Quantization

Model quantization represents a technique for model compression, vital in optimizing neural networks for resource-constrained environments. Quantization transforms the network's weights and activations from a floating-point to a low-bit representation, thereby reducing memory footprint and computational intensity. This transformation is quantitatively described as follows:

$$w_q = \text{c1amp}\left(\lfloor \frac{w}{s} \rfloor + z, 0, 2^b - 1\right), \quad (3)$$

$$\hat{w} = s \cdot (w_q - z) \approx w, \quad (4)$$

where w and \hat{w} denote the original and de-quantized weights or activations, w_q is the quantized integer representation, s represents the scaling factor, z is the zero point, and b is the bit precision corresponding to 2^b quantization levels. The uniform quantization here has equal intervals between each level. Quantization introduces an approximation (quantization) and a subsequent reconstruction (de-quantization) of network parameters.

Expanding upon uniform quantization, our research incorporates logarithmic quantizer that also aligns well with the hardware-oriented aspects. For instance log2 quantization, used primarily on positive activation values, is succinctly represented as:

$$w_q = \text{c1amp}\left(\lfloor -\log_2 \frac{w}{s} \rfloor, 0, 2^b - 1\right), \quad (5)$$

$$\hat{w} = s \cdot 2^{-w_q} \approx w. \quad (6)$$

This method, like uniform quantization, involves the scaling factor s but introduces a logarithmic approach to the quantization process. It offers rapid bit-shifting operations, making it a strategic choice for efficiently implementing models on hardware platforms. The integration of log2 quantization into our model framework further exemplifies our commitment to enhancing computational efficiency while maintaining fidelity in the intricate process of diffusion-based video generation.

3.3 Temporal Features in Video Diffusion Models

In the video diffusion model, the time step t is encoded by the function $h(\cdot)$ into a temporal encoding, which is then mapped to temporal features by the embedding function $f(\cdot)$. These temporal features are channel-adjusted by the function $g(\cdot)$ in every Resnet-block3D of the noise estimation network and fused with all frame features. Formally, for the i -th Resnetblock3D, this process can be described using the following equation:

$$\mathbf{F}_t = \mathbf{F} + g_i(f(h(t))), \quad (7)$$

where \mathbf{F}_t represents the frame feature fused with the projected temporal feature. We denote the temporal feature at time-step t as \mathbf{T}_{emb}^t :

$$\mathbf{T}_{emb}^t = f(h(t)). \quad (8)$$

4 MODIFICATIONS

4.1 High Temporal Discriminability Quantization

As previously discussed, video diffusion models introduce a frame dimension, which enables the model to predict the noise for N frame features in each inference, a concept illustrated in Figure 2. In contrast, in image diffusion models, the frame count remains fixed at one. Structurally, temporal features are integrated into the features of each frame, and the quantization noise consequently spreads across all frames. Features from different frames are further fused within the temporal attention blocks, which results in the effects of quantization being compounded. As indicated in Table 4, omitting the quantization of temporal features leads to a significant reduction in the FVD by 160.82 compared to the uniform baseline. These findings highlight the critical importance of precise temporal features for video diffusion models.

To further explore this, we investigate the temporal features to explain why uniform quantizers fail to function effectively. The distribution of temporal features demonstrates a pronounced skewness, with a majority of the values aggregating near zero, and outliers are several orders of magnitude greater than the typical values observed as depicted in Figure 4(a). Even with a 10-bit uniform quantizer, dense intervals utilize only one of the 1024 quantization levels, as depicted in Figure 4(b). This causes most values in the temporal features to collapse to a single value, as shown in Figure 3(b), severely impairing their distinguishability. The log2 quantizer, as shown in Figure 4(c), allocates more quantization levels to dense intervals, preserving the distribution of small values in the temporal features and thus their discriminability. As indicated in Table 4, the log quantizer reduces FVD by 131.63 compared to the linear quantizer, demonstrating its effectiveness. However, we note that despite the

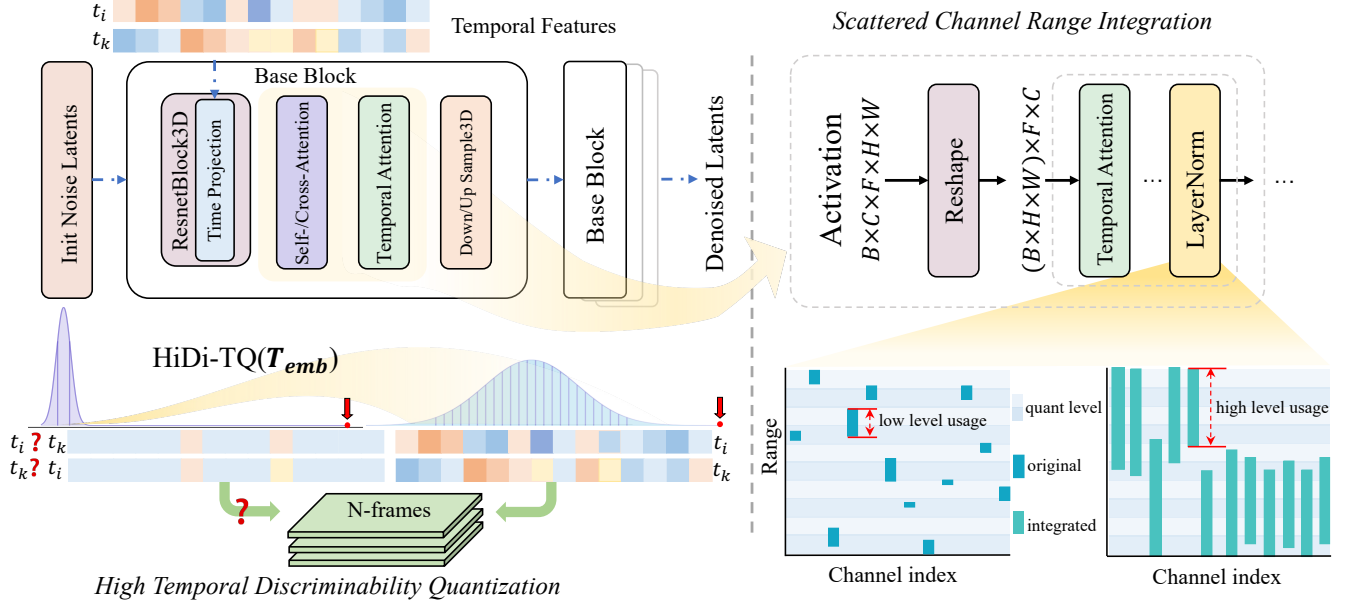


Figure 2: Overview of QVD. The left is the **High Temporal Discriminability Quantization**, which uses the **HiDi-TQ** quantizer to retain the low TDScore of temporal features. The red arrow points to the location of the outlier. The right is the **Scattered Channel Range Integration**, which aims at mitigating the discreteness and asymmetry in inter-channel activation ranges, thereby enhancing the utilization rate of quantization levels by individual channels.

improved FVD with the log quantizer, it incurs a greater L2 quantization loss compared to the uniform quantizer, as shown in Figure 5. We hypothesize that L2 loss prioritizes the impact of larger values while neglecting smaller values, which is inappropriate given the unique distribution.

We conduct comparative experiments to further validate the contribution of minor values to the discriminability of temporal features. Specifically, in setting 1, we zero the interval $[-0.5min, 0.5max]$, and in setting 2, we apply a noise mask ranging from $[-1.5, 1.5]$ to scale values within the $[0.9max, max]$ interval, where max and min denote the maximum and the minimum for the temporal feature, respectively. As detailed in Table 4, the model exhibited robustness to disturbances in large values, while homogenization of small values lead to a collapse in model performance, underscoring the critical importance of minor values in preserving the discriminability of temporal features.

This analysis indicates the necessity of designing a quantizer specifically for the unique distribution of temporal features and developing a metric to measure the discriminability of temporal features. Driven by the above motivations, we propose the **Temporal Discriminability Score (TDScore)** and **High Discriminability Quantizer for the Temporal Feature (HiDi-TQ)**.

4.1.1 Temporal Discriminability Score. The TDScore evaluates the similarity between the current temporal feature and several adjacent temporal features. We denote the discriminability score of the t -th temporal feature as $TDScore_t$. We initially apply a logarithmic function to \mathbf{T}_{emb}^t to enhance focus on minor values within the

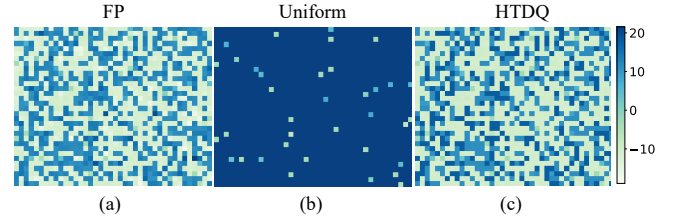


Figure 3: Heat maps of full-precision temporal feature and its quantized versions of the uniform quantizer and the HTDQ.

temporal feature as defined in Equation 9:

$$\mathbf{T}_{emb}^{t'} = \text{sign}(\mathbf{T}_{emb}^t) \cdot \left| \log_2 \|\mathbf{T}_{emb}^t\| \right|. \quad (9)$$

Subsequently, we compute the mean cosine similarity between the feature and its n contiguous time steps following Equation 10:

$$TDScore_t = \frac{1}{n} \sum_{i=t+1}^{i=t+n} \cos_sim(\mathbf{T}_{emb}^{t'}, \mathbf{T}_{emb}^{i'}). \quad (10)$$

A lower TDScore indicates higher discriminability of the temporal feature. We can employ the TDScore to assess the efficacy of quantization precisely.

4.1.2 High Discriminability Quantizer for Temporal Feature. As aforementioned, the quantization of temporal features not only necessitates minimizing quantization loss but also preserving distinctions between time steps. We evaluate quantizers calibrated using

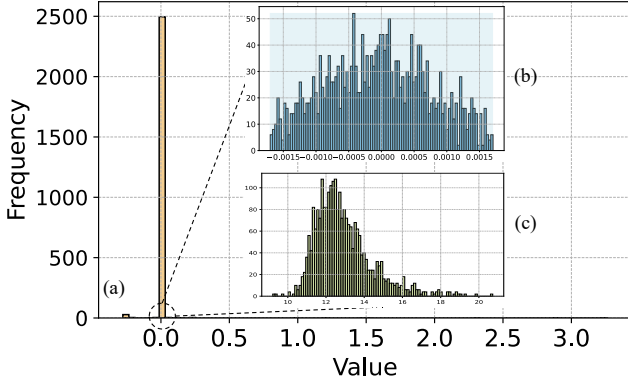


Figure 4: Histogram of the temporal feature. (a) shows the histogram of 100% data of a temporal feature. (b) presents the middle 90% of the data which is concentrated within the range of $[-0.002, 0.002]$ and a single blue rectangle in the background indicates that these data are mapped to the same value. (c) depicts the distribution of the middle 90% of data processed through a logarithmic function, covering 10 quantization levels.

min-max or mean squared error (MSE) calibration strategy, as illustrated in Figure 5. These quantizers minimize quantization loss but concurrently diminish the distinguishability of temporal features (TDScores are near 1). We introduce the high discriminability quantizer considering the unique distribution of temporal features. This quantizer is based on a logarithmic quantizer which is non-uniform. It allocates more quantization levels to values concentrated around zero, unlike uniform quantizers. Conversely, sparse distributions of large values are allocated fewer quantization levels. However, the vanilla logarithmic quantizer maps both the positive part and the negative part of temporal features to the same positive interval. This causes the data concentration regions of positive and negative intervals to overlap, exacerbating data concentration. Consequently, this reduces the utilization of available quantization levels. To address this issue, a relaxation coefficient β is introduced, as follows:

$$\mathbf{T}_{emb}^z = \text{sign}(\mathbf{T}_{emb}) \cdot \text{clip}\left(-\log_2 \frac{|\mathbf{T}_{emb} - \beta|}{s}, 0, 2^b - 1\right). \quad (11)$$

The quantization process is initiated by a β shift in the temporal features, thereby reducing the clustering of absolute values. \mathbf{T}_{emb}^z represents the quantized temporal features. The scaling factor s is typically set to be greater than the maximum absolute value of \mathbf{T}_{emb} to ensure that the scaled activation values fall within the range $[0, 1]$. Additionally, s can be adjusted to modify the data concentration, where increasing the value of s narrows the range of activation values and makes it more concentrated.

As illustrated in Figure 5, although the logarithmic quantizer ensures foundational temporal discrimination (low TDScore), it also incurs a considerable L2 loss (MSE loss). To balance the precision of quantization and temporal discrimination, we utilize a composite metric K as defined in Equation 12, which incorporates both

TDScore and L2 loss, to search the optimal s and β :

$$K = \sum_{i=1}^T TDScore_i + \sum_{i=1}^T (\mathbf{T}_{emb}^i - \hat{\mathbf{T}}_{emb}^i)^2. \quad (12)$$

The TDScore allows K to prioritize smaller values, while the L2 component ensures attention to losses in larger values. To mitigate truncation errors, We constrain the value of s to the interval

$$\left[\max(|\mathbf{T}_{emb}|), \frac{\min(|\mathbf{T}_{emb}|) + \text{eps}}{2^{1-2^n}} \right]. \quad (13)$$

This typically spans a very large range, to enhance search efficiency, we employ exponential step sizes where $s_i = \max|\mathbf{T}_{emb}| \times 2^{0.05 \times i}$.

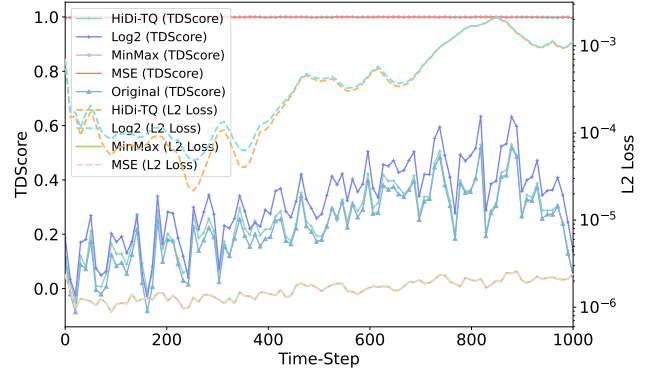


Figure 5: Performance of various quantization strategies. The left axis represents the TDScore. The right axis delineates the L2 quantization loss.

4.2 Scattered Channel Range Integration

Compared to the image diffusion models, we observe significant inter-channel variations in the video diffusion model. As depicted in Figure 1(b), we plot box plots for the activation sampled from the image diffusion model and output of the temporal attention block in the video diffusion model. It is evident that the activations generated by the temporal attention block exhibit discrete and asymmetric characteristics, referred to as inter-channel variations. The narrow range of individual channels leads to minimal overlap in the activation ranges across channels, resulting in low coverage of quantization levels per-channel, as illustrated in Figure 6, this diminishes the performance of the quantized model.

Unlike the issues previously identified in large language models (LLMs), the problem of inter-channel variations is particularly pronounced in video diffusion models. This issue differs significantly from the outliers extensively studied in LLMs. In LLMs, as indicated by OS+ [57], outliers manifest as extreme shifts in specific channels. These shifts are consistent across samples, which allows for the straightforward identification and adjustment of an accurate shift amount to align the channel midpoints. Such a method is effectively utilized in LLMs, where techniques like OS+ [57] align and scale channel midpoints in the activation of the Layer-Norm layer through a channel-wise shift to address these outliers. However, in video diffusion models, the challenge of inter-channel variations requires

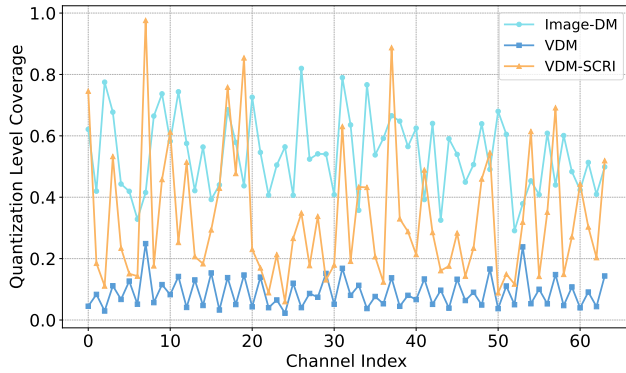


Figure 6: Quantization level coverage of activation sampled from the image and video diffusion models. It is defined as the ratio of each channel’s range to the overall range used for quantization. VDM-SCRI denotes the SCR-integrated version.

distinct approaches due to its more complex and variable nature compared to the channel-specific shifts observed in LLMs. Specifically, in video diffusion models, most channels exhibit varying degrees of shift that change with each sample, making it challenging to calculate an accurate shift for aligning the channel midpoints.

To address this issue, we propose the method of **Scattered Channel Range Integration (SCRI)**. Formally, SCRI is a straightforward approach, as illustrated in Equation 14:

$$\tilde{\mathbf{X}} = \mathbf{X} \oslash \mathbf{s}, \mathbf{s} = \frac{\mathbf{X}_{cmax}}{t}, \quad (14)$$

where \mathbf{X} denotes the activations with C channels, while \mathbf{s} , a vector of length C similar to that used in OS+ [57], is employed to adjust the range of activation values. \mathbf{X}_{cmax} represents a vector composed of the maximum activation values within each channel, and t serves as an adaptive parameter.

The SCRI, through meticulous design, can amplify the range of activation values for each channel, reducing discreteness and increasing overlap. However, an excessively large activation range is not conducive to improving the coverage of quantization levels for individual channels. To strike a balance between the activation range and the coverage of quantization levels, identifying the optimal value for s is essential. Specifically, through a forward pass, we use a calibration set to determine the maximum activations values \mathbf{X}_{cmax} . Concurrently, we determine the optimal t using a grid search approach, confining our search within $[\min(\mathbf{X}_{cmax}), \max(\mathbf{X}_{cmax})]$. The optimization criterion during this search is the minimization of the MSE loss, comparing the output of the quantized model block against that of the full-precision model, as follows:

$$\arg \min_t \|\mathcal{F}(\mathbf{W}, \mathbf{X}) - \mathcal{F}_Q(\mathbf{W}, \mathbf{X}; t)\|, \quad (15)$$

where \mathcal{F} represents the mapping function for the layers following LayerNorm in temporal attention modules and self-/cross-attention modules in the video diffusion model and \mathcal{F}_Q denotes the mapping function corresponding quantized module.

Specifically, we identify several layers to apply SCRI: the Feed Forward Network (FFN), the projection layer, typically a linear layer or a convolution layer, and the attention layer subsequent to the

Table 1: Quantization results on motion-guided video generation with TED-talks. * denotes our implementation according to open-source codes.

Method	Bits (W/A)	Size (Gb)	TBOPs	TED-Talks	
				FID-VID↓	FVD↓
Full Precision	32/32	22.8	9735	44.47	361.54
Linear Quant* [43]	8/8	5.7	716	80.70	618.33
PTQ4DM* [47]	8/8	5.7	716	77.55	590.89
Q-Diffusion* [33]	8/8	5.7	716	75.16	593.81
QVD	8/8	5.7	716	49.38	385.77
Linear Quant* [43]	6/8	4.3	555	82.43	649.02
PTQ4DM* [47]	6/8	4.3	555	84.40	644.42
Q-Diffusion* [33]	6/8	4.3	555	83.03	644.37
QVD	6/8	4.3	555	50.94	386.47
Linear Quant* [43]	6/6	4.3	430	119.02	1130.76
PTQ4DM* [47]	6/6	4.3	430	109.08	1074.93
Q-Diffusion* [33]	6/6	4.3	430	110.42	1006.69
QVD	6/6	4.3	430	77.54	683.72

LayerNorm. Similar to OS+ [57], we implement SCRI by making equivalent transformations to LayerNorm and subsequent layers, which incurs no additional overhead during inference. As depicted in Figure 6, SCRI significantly enhances the coverage of quantization levels by individual channels.

5 EXPERIMENTS

5.1 Implementation Details

Datasets and Quantization Settings. Video synthesis experiments are conducted on two cutting-edge models, MagicAnimate [60] and AnimateDiff [17], utilizing the TED-talks [48], FS-COCO [11] and COCO Captions [8] datasets. Both the input and output layers are consistently set at an 8-bit representation, whereas all remaining convolutional and linear layers are quantized in accordance with the predetermined target bit-width. To calibrate the models accurately, samples from all time steps of application (25 in this work) are collected to form a calibration set, corresponding to one video consisting of 16 consecutive frames. This process ensures that the models are finely tuned for generating high-quality video sequences, establishing a benchmark in the domain of video synthesis.

Evaluation Metrics. In our experimental framework, we report the spatiotemporal fidelity of video synthesis using the FID-VID [1] and FVD [52] metrics, combining image quality assessment through Fréchet Inception Distance with temporal coherence evaluation using Fréchet Video Distance. Following AnimateDiff [18], semantic integrity is evaluated using the CLIP metric [45], which leverages a sophisticated language-image pretraining model to measure the alignment between generated animations and reference imagery. This involves calculating the cosine similarity between CLIP image embeddings of each animation frame and reference images, thereby evaluating domain similarity (Domain). Furthermore, our assessment is enhanced by examining the similarity between the prompt embeddings and individual frames to assess text alignment (Text) and by analyzing the similarity between consecutive frames to evaluate motion smoothness (Smooth). For computational performance, we calculate Bit Operations (BOPs) [3, 19] per video diffusion model during each forward pass, balancing efficiency with processing demands.

Table 2: Quantization results on motion-guided and sketch-guided video generation with FS-COCO and COCO Captions, respectively. * denotes our implementation according to open-source codes.

Method	Bits (W/A)	Size (Gb)	TBOPs	FS-COCO			COCO Captions		
				CLIP-Metric			CLIP-Metric		
				Text.↑	Domain.↑	Smooth.↑	Text.↑	Domain.↑	Smooth.↑
Full Precision	32/32	22.8	9735	29.87	75.23	99.03	30.34	89.92	95.71
Linear Quant* [43]	8/8	5.7	716	28.05	69.40	98.68	30.00	84.97	92.80
PTQ4DM* [47]	8/8	5.7	716	28.23	70.92	98.46	29.61	83.88	91.49
Q-Diffusion* [33]	8/8	5.7	716	28.73	72.47	98.87	29.77	83.84	91.52
QVD	8/8	5.7	716	29.67	75.48	98.92	30.21	90.39	95.66
Linear Quant* [43]	6/8	4.3	555	28.19	69.59	98.77	29.93	83.80	91.92
PTQ4DM* [47]	6/8	4.3	555	28.96	71.39	98.48	29.93	83.13	90.62
Q-Diffusion* [33]	6/8	4.3	555	28.87	71.54	98.79	29.70	82.89	90.79
QVD	6/8	4.3	555	29.71	75.24	98.83	30.15	89.40	94.93
Linear Quant* [43]	6/6	4.3	430	26.32	64.52	96.35	29.24	78.51	91.91
PTQ4DM* [47]	6/6	4.3	430	27.83	68.43	96.12	27.98	72.83	89.58
Q-Diffusion* [33]	6/6	4.3	430	27.99	69.02	96.20	28.23	74.07	89.81
QVD	6/6	4.3	430	28.88	70.92	96.86	29.57	80.50	92.61

Table 3: The effect of different methods proposed in the paper on TED-talks.

Method	Bits (W/A)	FID-VID↓	FVD↓
Full Precision	32/32	44.47	361.54
Linear Quant (Baseline)	8/8	80.70	618.33
+ HTDQ	8/8	61.22	483.99
+ SCRI	8/8	67.57	529.70
QVD (HTDQ + SCRI)	8/8	49.38	385.77

Table 4: Detailed ablation of temporal features. † denotes using the full-precision temporal feature.

Method	Bits (W/A)	FID-VID↓	FVD↓
Full Precision	32/32	44.47	361.54
SCRI + Linear Quant	8/8	67.57	529.70
SCRI + Log2 Quant	8/8	50.43	398.07
SCRI + HTDQ	8/8	49.38	385.77
Linear Quant †	8/8	64.85	457.51
Linear Quant	8/8	80.70	618.33
perturbates outliers	8/8	65.94	487.91
perturbates values near zero	8/8	75.04	580.67

5.2 Main Results

Motion Guided. In this section, we apply our quantization method to the task of Human Image Animation, utilizing the MagicAnimate [60] framework on the TED-talks dataset [48]. MagicAnimate uses a motion sequence and a reference image to generate a video clip where the sequence directs the person’s movements. We use the plain round-to-nearest Linear Quantization [43], PTQ4DM [47] and Q-Diffusion [33] as our baselines. As shown in table 1, our QVD consistently outperforms other methods by a large margin. Actually, these methods specifically designed for image diffusion, namely PTQ4DM and Q-Diffusion, do not achieve significant performance improvements in video diffusion quantization. On the contrary, at W8A8, our QVD gains a FID-VID reduction of 25.78 (75.16→49.38 compared with Q-Diffusion) and a FVD reduction of 205.12 (590.89→385.77 compared with PTQ4DM) on TED-Talks, which is almost lossless. When the bit-width decreases (*i.e.*, W6A8 and W6A6), other methods drop drastically while our QVD maintains the performance to a great extent, merely introducing a 1.56 upswing in FID-VID and a 0.7 upswing in FVD.

Image-guided and Sketch-guided To demonstrate the superiority and versatility of our QVD, we further conducted experiments on AnimateDiff [18]. AnimateDiff utilizes both a visual modality (image or sketch) and a text prompt as inputs to generate videos. Our

Table 5: Detailed ablation of SCRI.

Method	Bits (W/A)	FID-VID↓	FVD↓
Full Precision	32/32	44.47	361.54
HTDQ + OS+ [57]	8/8	51.21	407.93
HTDQ + OS+ [57] without shift	8/8	50.48	405.16
HTDQ + SCRI	8/8	49.38	385.77

quantitative comparison mainly focuses on text alignment, domain similarity, and motion smoothness by employing the CLIP metric. Specifically, for the text alignment, our approach achieves a pioneering breakthrough on the FS-COCO dataset with Text-CLIP, surpassing 29 for the first time. For the domain similarity, Our QVD method leads the Q-Diffusion by 6.51 on the Domain-CLIP at W6A8 when evaluated on the COCO Captions dataset. For the motion smoothness, our method exhibits extraordinary video coherence on W8A8, remarkably achieving a score of only 0.05 lower than that of full precision (Smooth-CLIP).

5.3 Ablation Studies

In our ablation studies, we meticulously dissect the impact of each component in our QVD. These experiments are performed using

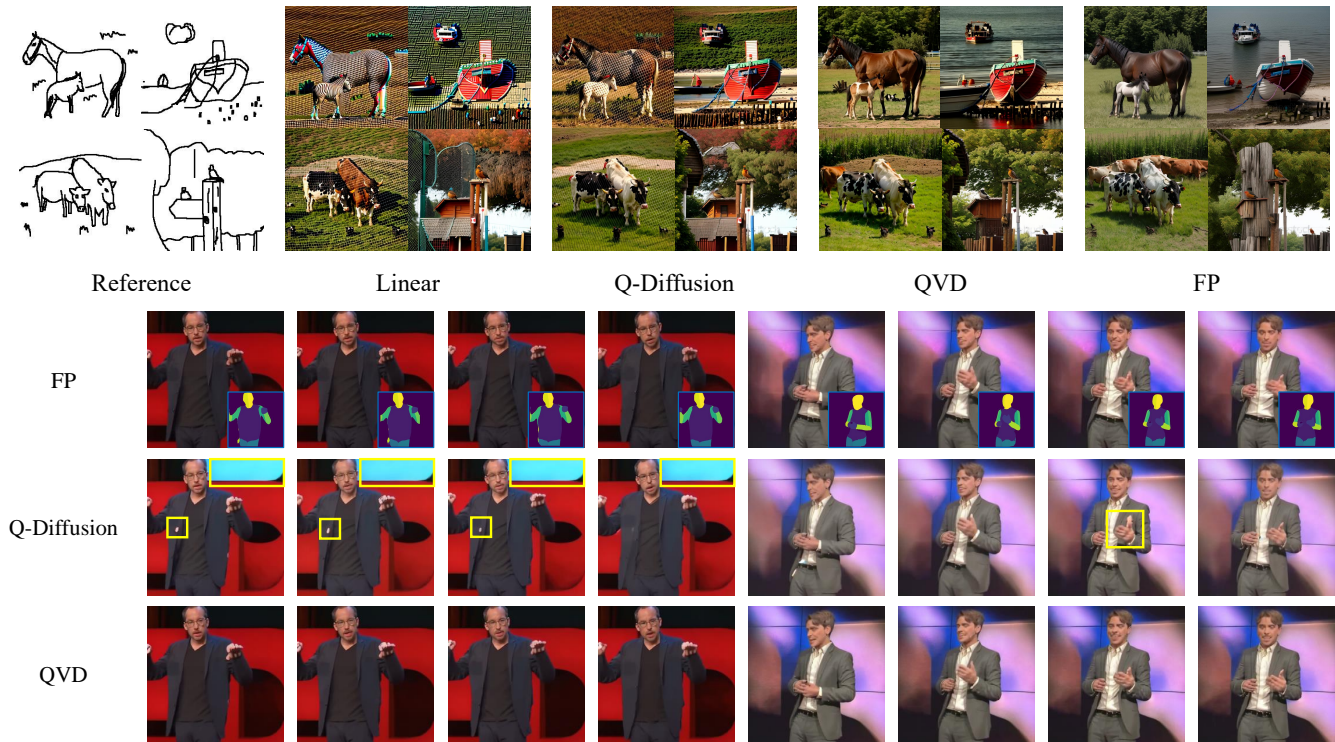


Figure 7: A comparison of generation samples between Q-Diffusion, QVD, and the full-precision model. The upper figure demonstrates the generative outcomes of AnimatedDiff, while the lower figure showcases the results from the Magic-Animate model.

Table 6: Different calibration settings for SCRI.

Frame	Time-step	FID-VID↓	FVD↓	Time-cost(s)
1	1	52.37	415.64	100.87
16	1	51.21	407.93	100.87
16	25	50.60	406.95	2534.51

the TED-talks dataset with W8A8 quantization, aiming to elucidate the individual contributions of different components to the overall effectiveness of the model. Linear quantization served as the baseline, adopting the MinMax calibration strategy for weight quantization and the MSE calibration strategy for activation quantization. Our analysis involves examining the effects of SCRI and HTDQ, as detailed in the following.

Overall Effect of HTDQ and SCRI. Table 3 outlines the collective impact of these components. The baseline model with linear quantization scores an FID-VID of 80.70 and an FVD of 618.33. Incorporating HTDQ remarkably improves these metrics to 61.22 and 483.99, respectively. Similarly, adding SCRI yields an improvement, achieving scores of 67.57 (FID-VID) and 529.70 (FVD). The combination of both HTDQ and SCRI (our complete Magic-animate model) further reduces these scores to 49.38 (FID-VID) and 385.77 (FVD), underlining the benefit of integrating both components.

Detailed Ablation of HTDQ. To dissect the influence of HTDQ, we consider two stages in its integration (Table 4): the log quantization and our enhanced HTDQ. The experimental data presented

in Table 4 clearly indicates the superiority of our enhanced HTDQ over the log quantization. When comparing the *SCRI+Log2 Quant* method and that with full *SCRI+HTDQ*, there is a noticeable improvement in both FID-VID and FVD scores, dropping from 50.43 to 49.38 for FID-VID, and from 398.07 to 385.77 for FVD. This demonstrates that our HTDQ, with its additional refinements, effectively enhances the quality of the quantized animations, offering a more faithful representation compared to the baseline.

Exploring the Impact of SCRI. In our ablation study detailed in Table 5, we compare the impact of different scaling methods on quantization quality. When the shift operation is removed from the OS+ [57] method, we see a modest improvement in both FID-VID (reduced from 51.21 to 50.48) and FVD (lowered from 407.93 to 405.16). Further refining the scale computation in our SCRI method yields even better results, with a notable decrease in FID-VID to 49.38 and FVD to 385.77, demonstrating the effectiveness of our adjustments in scale calculation for quantization.

Investigating Calibration Efficiency. To enhance the efficiency of the search process of SCRI, we investigate the impact of varying the number of frames and time steps on the calibration outcomes. As shown in Table 6, a calibration setup using 16 frame features and 1 time-step achieves a balance between performance and time efficiency. All the experiments are conducted based on this setup.

5.4 Comparison of Visualization Results

Figure 7 shows the W8A8 qualitative results on FS-COCO and TED-talks datasets. When the reference is sketch (top), Linear Quantization and Q-Diffusion exhibit grid-like artifacts in their prediction results, while QVD successfully eliminates this issue and more closely approximates the performance of a full-precision model. When the reference is the motion video (bottom), Q-Diffusion generates noise and disordered backgrounds in its outputs. Moreover, QVD demonstrates superior detail retention for moving objects, exemplified by the hand of the speaker in the lower right corner.

6 CONCLUSION

In this work, we explore the application of post-training quantization in video diffusion models. We identify the significance of distinctive features for high-quality video generation and introduce the HTDQ method to preserve the discriminability of temporal features after quantization. Additionally, we observed a severe inter-channel variation issue in video diffusion models. To address this, we proposed the SCRI method to integrate activations across channels, thereby enhancing the performance of the quantized model. Our proposed QVD quantization framework is the first to quantize video diffusion models to 8-bit without significant performance degradation.

REFERENCES

- [1] Yogesh Balaji, Martin Renqiang Min, Bing Bai, Rama Chellappa, and Hans Peter Graf. 2019. Conditional GAN with Discriminative Filter Generation for Text-to-Video Synthesis. In *IJCAI*, Vol. 1. 2.
- [2] Fan Bao, Chongxuan Li, Jun Zhu, and Bo Zhang. 2022. Analytic-dpm: an analytic estimate of the optimal reverse variance in diffusion probabilistic models. *arXiv preprint arXiv:2201.06503* (2022).
- [3] Chaim Baskin, Natan Liss, Eli Schwartz, Evgenii Zheltonozhskii, Raja Giryes, Alex M. Bronstein, and Avi Mendelson. 2019. UNIQ: Uniform Noise Injection for Non-Uniform Quantization of Neural Networks. *ACM Transactions on Computer Systems* 37, 1–4 (Nov. 2019), 1–15. <https://doi.org/10.1145/3444943>
- [4] Andreas Blattmann, Tim Dockhorn, Sumith Kulal, Daniel Mendelevitch, Maciej Kilian, Dominik Lorenz, Yam Levi, Zion English, Vikram Voleti, Adam Letts, et al. 2023. Stable video diffusion: Scaling latent video diffusion models to large datasets. *arXiv preprint arXiv:2311.15127* (2023).
- [5] Andreas Blattmann, Robin Rombach, Huan Ling, Tim Dockhorn, Seung Wook Kim, Sanja Fidler, and Karsten Kreis. 2023. Align your latents: High-resolution video synthesis with latent diffusion models. In *Proceedings of the IEEE/CVF Conference on Computer Vision and Pattern Recognition*. 22563–22575.
- [6] Hong Chen, Chengtao Lv, Liang Ding, Haotong Qin, Xiabin Zhou, Yifu Ding, Xuebo Liu, Min Zhang, Jinyang Guo, Xianglong Liu, et al. 2024. DB-LLM: Accurate Dual-Binarization for Efficient LLMs. *arXiv preprint arXiv:2402.11960* (2024).
- [7] Tsai-Shien Chen, Chieh Hubert Lin, Hung-Yu Tseng, Tsung-Yi Lin, and Ming-Hsuan Yang. 2023. Motion-conditioned diffusion model for controllable video synthesis. *arXiv preprint arXiv:2304.14404* (2023).
- [8] Xinlei Chen, Hao Fang, Tsung-Yi Lin, Ramakrishna Vedantam, Saurabh Gupta, Piotr Dollar, and C. Lawrence Zitnick. 2015. Microsoft COCO Captions: Data Collection and Evaluation Server. [arXiv:1504.00325](https://arxiv.org/abs/1504.00325) [cs.CV]
- [9] Jungwook Choi, Zhuo Wang, Swagath Venkataramani, Pierce I-Jen Chuang, Vijayalakshmi Srinivasan, and Kailash Gopalakrishnan. 2018. Pact: Parameterized clipping activation for quantized neural networks. *arXiv preprint arXiv:1805.06085* (2018).
- [10] Yoni Choukroun, Eli Kravchik, Fan Yang, and Pavel Kisilev. 2019. Low-bit quantization of neural networks for efficient inference. In *2019 IEEE/CVF International Conference on Computer Vision Workshop (ICCVW)*. IEEE, 3009–3018.
- [11] Pinaki Nath Chowdhury, Aneeshan Sain, Ayan Kumar Bhunia, Tao Xiang, Yulia Gryaditskaya, and Yi-Zhe Song. 2022. Fs-coco: Towards understanding of freehand sketches of common objects in context. In *European Conference on Computer Vision*. Springer, 253–270.
- [12] Özgün Çiçek, Ahmed Abdulkadir, Soeren S Lienkamp, Thomas Brox, and Olaf Ronneberger. 2016. 3D U-Net: learning dense volumetric segmentation from sparse annotation. In *Medical Image Computing and Computer-Assisted Intervention—MICCAI 2016: 19th International Conference, Athens, Greece, October 17–21, 2016, Proceedings, Part II 19*. Springer, 424–432.
- [13] Antonia Creswell, Tom White, Vincent Dumoulin, Kai Arulkumaran, Biswa Sen-gupta, and Anil A Bharath. 2018. Generative adversarial networks: An overview. *IEEE signal processing magazine* 35, 1 (2018), 53–65.
- [14] Patrick Esser, Johnathan Chiu, Parmida Atighehchian, Jonathan Granskog, and Anastasis Germanidis. 2023. Structure and content-guided video synthesis with diffusion models. In *Proceedings of the IEEE/CVF International Conference on Computer Vision*. 7346–7356.
- [15] Steven K Esser, Jeffrey L McKinstry, Deepika Bablani, Rathinakumar Appuswamy, and Dharmendra S Modha. 2019. Learned step size quantization. *arXiv preprint arXiv:1902.08153* (2019).
- [16] Gongfan Fang, Xinyin Ma, and Xinchao Wang. 2024. Structural pruning for diffusion models. *Advances in neural information processing systems* 36 (2024).
- [17] Yuwei Guo, Ceyuan Yang, Anyi Rao, Maneesh Agrawala, Dahua Lin, and Bo Dai. 2023. Sparsctrl: Adding sparse controls to text-to-video diffusion models. *arXiv preprint arXiv:2311.16933* (2023).
- [18] Yuwei Guo, Ceyuan Yang, Anyi Rao, Zhengyang Liang, Yaohui Wang, Yu Qiao, Maneesh Agrawala, Dahua Lin, and Bo Dai. 2024. AnimateDiff: Animate Your Personalized Text-to-Image Diffusion Models without Specific Tuning. [arXiv:2307.04725](https://arxiv.org/abs/2307.04725) [cs.CV]
- [19] Yefei He, Luping Liu, Jing Liu, Weijia Wu, Hong Zhou, and Bohan Zhuang. 2024. Ptdq: Accurate post-training quantization for diffusion models. *Advances in Neural Information Processing Systems* 36 (2024).
- [20] Yingqing He, Menghan Xia, Haoxin Chen, Xiaodong Cun, Yuan Gong, Jinbo Xing, Yong Zhang, Xintao Wang, Chao Weng, Ying Shan, et al. 2023. Animate-a-story: Storytelling with retrieval-augmented video generation. *arXiv preprint arXiv:2307.06940* (2023).
- [21] Yingqing He, Tianyu Yang, Yong Zhang, Ying Shan, and Qifeng Chen. 2022. Latent video diffusion models for high-fidelity long video generation. *arXiv preprint arXiv:2211.13221* (2022).
- [22] Jonathan Ho, Ajay Jain, and Pieter Abbeel. 2020. Denoising diffusion probabilistic models. *Advances in neural information processing systems* 33 (2020), 6840–6851.
- [23] Jonathan Ho, Tim Salimans, Alexey Gritsenko, William Chan, Mohammad Norouzi, and David J Fleet. 2022. Video diffusion models. *Advances in Neural Information Processing Systems* 35 (2022), 8633–8646.
- [24] Edward J Hu, Yelong Shen, Phillip Wallis, Zeyuan Allen-Zhu, Yuanzhi Li, Shean Wang, Lu Wang, and Weizhu Chen. 2021. Lora: Low-rank adaptation of large language models. *arXiv preprint arXiv:2106.09685* (2021).
- [25] Li Hu, Xin Gao, Peng Zhang, Ke Sun, Bang Zhang, and Lifeng Bo. 2023. Animate anyone: Consistent and controllable image-to-video synthesis for character animation. *arXiv preprint arXiv:2311.17117* (2023).
- [26] Yaosi Hu, Zhenzhong Chen, and Chong Luo. 2023. Lamd: Latent motion diffusion for video generation. *arXiv preprint arXiv:2304.11603* (2023).
- [27] Yushi Huang, Ruihao Gong, Jing Liu, Tianlong Chen, and Xianglong Liu. 2023. Tfmq-dm: Temporal feature maintenance quantization for diffusion models. *arXiv preprint arXiv:2311.16503* (2023).
- [28] Benoit Jacob, Skirmantas Kligys, Bo Chen, Menglong Zhu, Matthew Tang, Andrew Howard, Hartwig Adam, and Dmitry Kalenichenko. 2018. Quantization and training of neural networks for efficient integer-arithmetic-only inference. In *Proceedings of the IEEE conference on computer vision and pattern recognition*. 2704–2713.
- [29] Johanna Karras, Aleksander Holynski, Ting-Chun Wang, and Ira Kemelmacher-Shlizerman. 2023. Dreampose: Fashion image-to-video synthesis via stable diffusion. In *2023 IEEE/CVF International Conference on Computer Vision (ICCV)*. IEEE, 22623–22633.
- [30] Sanghyun Kim, Seohyeon Jung, Balhae Kim, Moonseok Choi, Jinwoo Shin, and Juho Lee. 2023. Towards safe self-distillation of internet-scale text-to-image diffusion models. *arXiv preprint arXiv:2307.05977* (2023).
- [31] Seungwoo Lee, Chaerin Kong, Donghyeon Jeon, and Nojun Kwak. 2023. AADiff: Audio-Aligned Video Synthesis with Text-to-Image Diffusion. *arXiv preprint arXiv:2305.04001* (2023).
- [32] Muyang Li, Ji Lin, Chenlin Meng, Stefano Ermon, Song Han, and Jun-Yan Zhu. 2022. Efficient spatially sparse inference for conditional gans and diffusion models. *Advances in Neural Information Processing Systems* 35 (2022), 28858–28873.
- [33] Xiuyu Li, Yijiang Liu, Long Lian, Huanrui Yang, Zhen Dong, Daniel Kang, Shanghang Zhang, and Kurt Keutzer. 2023. Q-diffusion: Quantizing diffusion models. In *Proceedings of the IEEE/CVF International Conference on Computer Vision*. 17535–17545.
- [34] Yuhang Li, Ruihao Gong, Xu Tan, Yang Yang, Peng Hu, Qi Zhang, Fengwei Yu, Wei Wang, and Shi Gu. 2021. Breq: Pushing the limit of post-training quantization by block reconstruction. *arXiv preprint arXiv:2102.05426* (2021).
- [35] Luping Liu, Yi Ren, Zhijie Lin, and Zhou Zhao. 2022. Pseudo numerical methods for diffusion models on manifolds. *arXiv preprint arXiv:2202.09778* (2022).
- [36] Vivian Liu, Tao Long, Nathan Raw, and Lydia Chilton. 2023. Generative disco: Text-to-video generation for music visualization. *arXiv preprint arXiv:2304.08551* (2023).
- [37] Cheng Lu, Yuhao Zhou, Fan Bao, Jianfei Chen, Chongxuan Li, and Jun Zhu. 2022. Dpm-solver: A fast ode solver for diffusion probabilistic model sampling in

- around 10 steps. *Advances in Neural Information Processing Systems* 35 (2022), 5775–5787.
- [38] Yue Ma, Yingqing He, Xiaodong Cun, Xintao Wang, Ying Shan, Xiu Li, and Qifeng Chen. 2023. Follow your pose: Pose-guided text-to-video generation using pose-free videos. *arXiv preprint arXiv:2304.01186* (2023).
- [39] Chenlin Meng, Robin Rombach, Ruiqi Gao, Diederik Kingma, Stefano Ermon, Jonathan Ho, and Tim Salimans. 2023. On distillation of guided diffusion models. In *Proceedings of the IEEE/CVF Conference on Computer Vision and Pattern Recognition*. 14297–14306.
- [40] Daisuke Miyashita, Edward H Lee, and Boris Murmann. 2016. Convolutional neural networks using logarithmic data representation. *arXiv preprint arXiv:1603.01025* (2016).
- [41] Eyal Molad, Eliahu Horwitz, Dani Valevski, Alex Rav Acha, Yossi Matias, Yael Pritch, Yaniv Leviathan, and Yedid Hoshen. 2023. Dreamix: Video diffusion models are general video editors. *arXiv preprint arXiv:2302.01329* (2023).
- [42] Markus Nagel, Rana Ali Amjad, Mart Van Baalen, Christos Louizos, and Tijmen Blankevoort. 2020. Up or down? adaptive rounding for post-training quantization. In *International Conference on Machine Learning*. PMLR, 7197–7206.
- [43] Markus Nagel, Marios Fournarakis, Rana Ali Amjad, Yelysei Bondarenko, Mart Van Baalen, and Tijmen Blankevoort. 2021. A white paper on neural network quantization. *arXiv preprint arXiv:2106.08295* (2021).
- [44] Haomiao Ni, Changhao Shi, Kai Li, Sharon X Huang, and Martin Renqiang Min. 2023. Conditional image-to-video generation with latent flow diffusion models. In *Proceedings of the IEEE/CVF Conference on Computer Vision and Pattern Recognition*. 18444–18455.
- [45] Alec Radford, Jong Wook Kim, Chris Hallacy, Aditya Ramesh, Gabriel Goh, Sandhini Agarwal, Girish Sastry, Amanda Askell, Pamela Mishkin, Jack Clark, et al. 2021. Learning transferable visual models from natural language supervision. In *International conference on machine learning*. PMLR, 8748–8763.
- [46] Robin Rombach, Andreas Blattmann, Dominik Lorenz, Patrick Esser, and Björn Ommer. 2022. High-resolution image synthesis with latent diffusion models. In *Proceedings of the IEEE/CVF conference on computer vision and pattern recognition*. 10684–10695.
- [47] Yuzhang Shang, Zhihang Yuan, Bin Xie, Bingzhe Wu, and Yan Yan. 2023. Post-training quantization on diffusion models. In *Proceedings of the IEEE/CVF Conference on Computer Vision and Pattern Recognition*. 1972–1981.
- [48] Aliaksandr Siarohin, Oliver J Woodford, Jian Ren, Menglei Chai, and Sergey Tulyakov. 2021. Motion representations for articulated animation. In *Proceedings of the IEEE/CVF Conference on Computer Vision and Pattern Recognition*. 13653–13662.
- [49] Junhyuk So, Jungwon Lee, Daehyun Ahn, Hyungjun Kim, and Eunhyeok Park. 2024. Temporal dynamic quantization for diffusion models. *Advances in Neural Information Processing Systems* 36 (2024).
- [50] Jascha Sohl-Dickstein, Eric Weiss, Niru Maheswaranathan, and Surya Ganguli. 2015. Deep unsupervised learning using nonequilibrium thermodynamics. In *International conference on machine learning*. PMLR, 2256–2265.
- [51] Jiaming Song, Chenlin Meng, and Stefano Ermon. 2020. Denoising diffusion implicit models. *arXiv preprint arXiv:2010.02502* (2020).
- [52] Thomas Unterthiner, Sjoerd Van Steenkiste, Karol Kurach, Raphael Marinier, Marcin Michalski, and Sylvain Gelly. 2018. Towards accurate generative models of video: A new metric & challenges. *arXiv preprint arXiv:1812.01717* (2018).
- [53] Tan Wang, Linjie Li, Kevin Lin, Yuanhao Zhai, Chung-Ching Lin, Zhengyuan Yang, Hanwang Zhang, Zicheng Liu, and Lijuan Wang. 2023. Disco: Disentangled control for realistic human dance generation. *arXiv preprint arXiv:2307.00040* (2023).
- [54] Xiang Wang, Hangjie Yuan, Shiwei Zhang, Dayou Chen, Jiuniu Wang, Yingya Zhang, Yujun Shen, Deli Zhao, and Jingren Zhou. 2024. Videocomposer: Compositional video synthesis with motion controllability. *Advances in Neural Information Processing Systems* 36 (2024).
- [55] Yaohui Wang, Xinyuan Chen, Xin Ma, Shangchen Zhou, Ziqi Huang, Yi Wang, Ceyuan Yang, Yanan He, Jiashuo Yu, Peiqing Yang, et al. 2023. Lavie: High-quality video generation with cascaded latent diffusion models. *arXiv preprint arXiv:2309.15103* (2023).
- [56] Xiuying Wei, Ruihao Gong, Yuhang Li, Xianglong Liu, and Fengwei Yu. 2022. Qdrop: Randomly dropping quantization for extremely low-bit post-training quantization. *arXiv preprint arXiv:2203.05740* (2022).
- [57] Xiuying Wei, Yunchen Zhang, Yuhang Li, Xiangguo Zhang, Ruihao Gong, Jinyang Guo, and Xianglong Liu. 2023. Outlier suppression+: Accurate quantization of large language models by equivalent and optimal shifting and scaling. *arXiv preprint arXiv:2304.09145* (2023).
- [58] Hao Wu, Patrick Judd, Xiaojie Zhang, Mikhail Isaev, and Paulius Micikevicius. 2020. Integer quantization for deep learning inference: Principles and empirical evaluation. *arXiv preprint arXiv:2004.09602* (2020).
- [59] Jay Zhangjie Wu, Yixiao Ge, Xintao Wang, Stan Weixian Lei, Yuchao Gu, Yufei Shi, Wynne Hsu, Ying Shan, Xiaoju Qie, and Mike Zheng Shou. 2023. Tune-a-video: One-shot tuning of image diffusion models for text-to-video generation. In *Proceedings of the IEEE/CVF International Conference on Computer Vision*. 7623–7633.
- [60] Zhongcong Xu, Jianfeng Zhang, Jun Hao Liew, Hanshu Yan, Jia-Wei Liu, Chenxu Zhang, Jiashi Feng, and Mike Zheng Shou. 2023. MagicAnimate: Temporally Consistent Human Image Animation using Diffusion Model. arXiv:2311.16498 [cs.CV]
- [61] Shengming Yin, Chenfei Wu, Jian Liang, Jie Shi, Houqiang Li, Gong Ming, and Nan Duan. 2023. Dragnuwa: Fine-grained control in video generation by integrating text, image, and trajectory. *arXiv preprint arXiv:2308.08089* (2023).
- [62] David Junhao Zhang, Jay Zhangjie Wu, Jia-Wei Liu, Rui Zhao, Lingmin Ran, Yuchao Gu, Difei Gao, and Mike Zheng Shou. 2023. Show-1: Marrying pixel and latent diffusion models for text-to-video generation. *arXiv preprint arXiv:2309.15818* (2023).
- [63] Qinsheng Zhang, Molei Tao, and Yongxin Chen. 2022. gddim: Generalized denoising diffusion implicit models. *arXiv preprint arXiv:2206.05564* (2022).
- [64] Daquan Zhou, Weimin Wang, Hanshu Yan, Weiwei Lv, Yizhe Zhu, and Jiashi Feng. 2022. Magicvideo: Efficient video generation with latent diffusion models. *arXiv preprint arXiv:2211.11018* (2022).
- [65] Junchen Zhu, Huan Yang, Huiguo He, Wenjing Wang, Zixi Tuo, Wen-Huang Cheng, Lianli Gao, Jingkuan Song, and Jianlong Fu. 2023. Moviefactory: Automatic movie creation from text using large generative models for language and images. In *Proceedings of the 31st ACM International Conference on Multimedia*. 9313–9319.